

# We are IntechOpen, the world's leading publisher of Open Access books Built by scientists, for scientists

6,900

Open access books available

186,000

International authors and editors

200M

Downloads

Our authors are among the

154

Countries delivered to

TOP 1%

most cited scientists

12.2%

Contributors from top 500 universities



WEB OF SCIENCE™

Selection of our books indexed in the Book Citation Index  
in Web of Science™ Core Collection (BKCI)

Interested in publishing with us?  
Contact [book.department@intechopen.com](mailto:book.department@intechopen.com)

Numbers displayed above are based on latest data collected.  
For more information visit [www.intechopen.com](http://www.intechopen.com)



# Functional Capabilities of Coupled Memristor-Based Reactance-Less Oscillators

*Vladimir V. Rakitin and Sergey G. Rusakov*

## Abstract

New functionalities of reactance-less memristor based oscillators are discussed which arise when two elementary oscillators are connected. It is shown that the system of coupled memristor based oscillators can be used for converting analog and analog-digital signals into binary pulse sequences. The approach to control the thresholds in memristor based oscillators is discussed. Standard control approach in memristor based oscillators is the exploitation of input signal to drive the rate of change in the state of the memristor. In contrast, the main idea of the considered controlling approach is to send the input signal not directly to the memristor device but to the comparator circuit and as result to control oscillator circuit behavior by change of interval of memristor resistor variation. The capabilities of coupled memristor based oscillators with control thresholds are sufficient for constructing the simple circuit elements of oscillatory computing architectures.

**Keywords:** reactance-less memristor based oscillators, coupling oscillators, memristor devices, threshold comparator, switching thresholds, binary oscillator networks

## 1. Introduction

The simplicity of the design of memristor based circuits and the possibility of manufacturing memristors [1–3] using integrated technology make them promising for use in a variety of information storage and processing systems. The construction of neuromorphic systems [4–8] is one of the most important memristor applications where the memristors provide the function of nonvolatile analog memory.

Due to memristor capabilities the wide implementation of memristors is predicted in different circuit application spheres including analog circuits. The properties of memristors [3, 9] open up new possibilities of constructing the memristor based oscillators (MBO) of different types [10–14]. The complex behavior of MBOs is analyzed in some papers (see for instance [15–18]). The inertial property of memristors provides the elimination from oscillator circuits the reactive elements (inductors and capacitors) which are poorly compatible with the requirements of the integrated implementation of neuromorphic systems. By the present time the various types of reactance-less MBO have been proposed [19–28]. This class of oscillators is considered below in the paper.

The neuromorphic systems including artificial neurons (AN) and networks become promising area where the analog memory plays the important role [29–39].

The memory elements are located between neurons and provide restructuring the coupling weight coefficients. Memristors are well suited to the requirements for artificial synapses [9, 40, 41]. The memristor resistance determines the value of the weight coefficients. The change in resistance under the action of current determines the possibility of restructuring the connections.

However, it should be noted that the properties of memristors allow them to be used not only as synaptic elements but also in the artificial neurons themselves. It can be mentioned that the reactance-less MBO consisting of memristor device and an active element, for instance comparator, can be also considered as simple AN model. Such an oscillator element can be inhibited or excited similarly to AN behavior. Its state can be specified by the phase of periodic oscillation.

Advanced AN models [8] that more accurately describe the behavior of biological neurons have high complexity to represent essentially more complex and various dynamical processes. The response of oscillatory AN to the input excitation involves not only changing the state but also changing the character of generation of output pulse train. In this case the number of the pulses and position of the pulses in pulse train depend on input amplitude and transient prehistory.

The complex mathematical model is required to represent such a behavior. This is usually achieved by increasing the order of the model. The complexity of circuits of corresponding oscillatory AN is also must be increased [42, 43] and strict requirements for the precision of circuit parameters must be met.

We present the alternative approach in this paper. We demonstrate that coupled memristor-based reactance-less oscillators have the set of modes with dynamical processes that is enough to provide the desired complex behavior. To support these capabilities at circuit level the approach to MBO construction is presented that based on controlling the comparator threshold. Some advantages of this approach are demonstrated.

Among the advantages of controlling threshold approach in MBO it is essential to point out the opportunity to construct piecewise constant (PWC) oscillators. Recently AN models based on piecewise constant (PWC) oscillators have appeared [44–46]. Such AN models are convenient in practice. PWC oscillators are the oscillators with mathematical models which are systems of ordinary differential equations (ODE) with piecewise constant coefficients. The signals generated by AN in this case are piecewise linear functions of time. PWC oscillators are developed on the base of standard electronic components including amplifiers, logic gates, resistors, capacitors. The transient processes occur in these circuits under constant excitation, for example the charge or discharge of the capacitor at constant current. The analysis of AN behavior of such type and networks based on them is given in papers [47, 48]. The nonlinearity of the memristor characteristics due to the change in its resistance when current flows through device limits the development of PWC memristor based oscillators [49, 50]. Application of the considered approach to control threshold in MBO avoids this restriction because it provides use only changing the sign of the current through the memristor while generation process.

Application in binary oscillator networks is other important capability of the considered coupled reactance-less MBOs. Oscillatory neural networks are promising candidates for solving a number of complex computational problems [51–55]. The most suitable circuit elements for such networks are binary generators with binary output signals [56–58]. In binary oscillator networks (BON) binary signals are exchanged and information is represented by binary streams. The considered coupled reactance-less MBOs can be applied as elementary binary oscillators.

The rest of the paper is organized as follows. Section 2 presents the principle of controlling thresholds in MBO circuits. The circuit version of coupled MBOs with positive couplings and its functionalities are discussed in Section 3. In Section 4 the

functional capabilities of coupled MBOs with inverting connections are given. The main properties of coupled MBO for use in binary generator networks are considered in Section 5. The technique of using phase planes to analyze the behavior of MBOs is widely used in sections.

2. Foundation: the principle of controlling threshold parameters in memristor based oscillator circuits

2.1 Operating principles of reactance-less memristor based oscillators

Oscillators without inductors and capacitors are the result of the memristor features applying. The self-excitation conditions are provided by the inertia of the resistance change of memristors when current flows through memristors devices. The absence of reactive elements allows to minimize the size of memristor based oscillators (MBO). The requirements to oscillator-based computing are met, in particular, by various variants of MBOs that differ in the number of memristor devices and the techniques of their coupling.

The schematic of typical reactance-less MBO is shown in **Figure 1a**. The circuit consists of memristor device  $M$  and a two-threshold comparator (TTC) with a current generator. The comparator converts the voltage  $v$  on the memristor to a binary output signal  $v_{out}$  (**Figure 1b**). The current generator converts the output binary signal ("0" and "1") of  $v_{out}$  to opposite corresponding currents  $i(v)$  ( $-I$  and  $+I$ ). The current input  $i_{in}$  is conventional input for reactance-less MBO. The memristor is connected to the input of the comparator by anode.

The memristor resistance  $R$  is decreased at a positive voltage  $v$  at anode when a positive current  $i$  flows in. The transfer function of the comparator is shown in **Figure 1b**. The comparator output voltage is "0" at  $-V_M < v < V_m$  and it is equal to

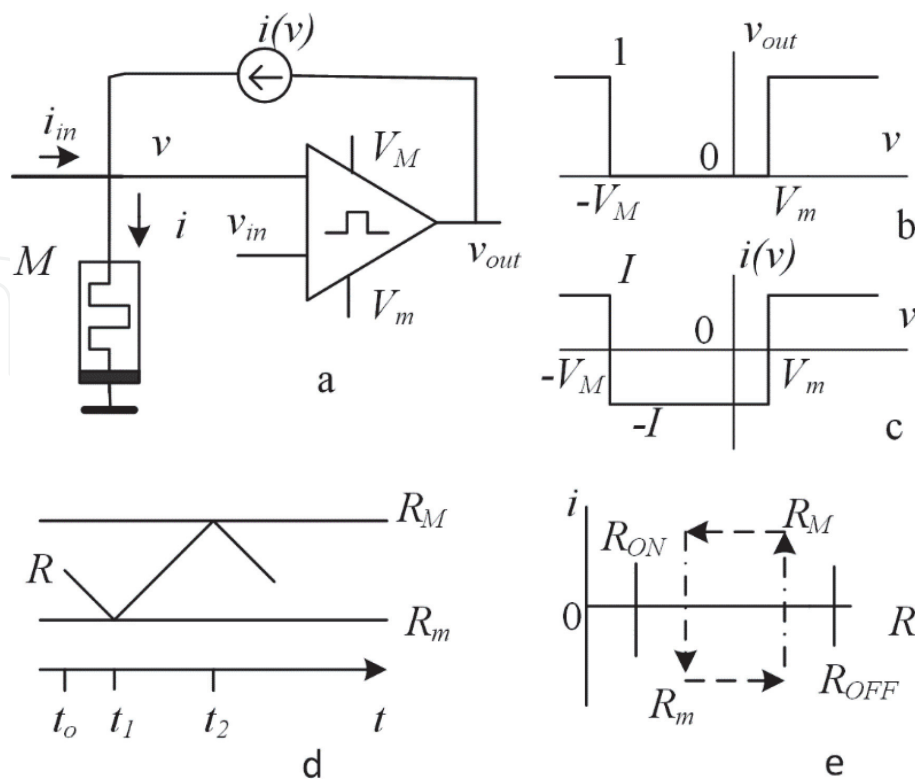


**Figure 1.** Typical illustrative graphs of behavior of reactance-less memristor based oscillator: (a) schematic of memristor based oscillator), (b) transfer function of comparator, (c) input function of comparator with current source, (d) waveforms of varying memristor resistor, (e) hysteresis loop for memristor resistor at phase plane.

“1” otherwise. Here  $V_M > V_m$ . The current generator in the negative feedback circuit of the comparator converts the binary output signal (“0”, “1”) into a negative current and a positive current through the memristor ( $-I$ ,  $+I$ ), respectively (**Figure 1c**). The input current  $i_{in}$  is summed with the current  $i(v)$ .

The memristor resistance can be considered as characteristic of oscillator state. Typical graph of varying memristor resistance in self-excitation mode of oscillator is given in **Figure 1d**. The phase plan (**Figure 1e**) illustrates the cycle of change of the memristor resistance  $R$  while oscillations as hysteresis loop.

Let us consider the cycle of periodic self-excitation mode of memristor oscillator (**Figure 1a**). Let's assume that for the initial moment of time  $t_0$  the voltage value  $v$  is  $v > V_m$  (**Figure 1c**). In this case the current is positive  $i = I$  and  $v_{out} = "1"$ . Therefore, the memristor resistance  $R$  and the memristor voltage are reduced. At time  $t_1$  the voltage reaches the threshold value  $v = V_m$ , the output voltage  $v_{out}$  goes from state “1” to state “0”. The value of memristor resistance is  $R_m = V_m/I$  at this time point. Here  $R_m$  is lower threshold value of the memristor resistance. In this case current  $i$  and voltage  $v$  become negative:  $i = -I$  and  $v = -V_m$ . The memristor resistance begin to increase, this leads to decreasing the negative voltage on the memristor. At time  $t_2$  it reaches the value  $v = -V_M$ , the output of the comparator goes from “0” to “1”, the current and voltage on the memristor become positive again:  $i = I$ ,  $v = V_M$ . At this time point, the resistance of the memristor achieves the value  $R_M = V_M/I$  where  $R_M$  is upper threshold resistance value. To provide periodicity of this process the following conditions must be satisfied

$$R_{ON} < R_m = \frac{V_m}{I} < \frac{V_M}{I} = R_M < R_{OFF}. \quad (1)$$

Here  $R_{ON}$  - is the minimal memristor resistance,  $R_{OFF}$  - is the maximal memristor resistance. In this case, the memristor resistance will periodically change in the range from the lower threshold value  $R_m$  to the upper threshold resistance  $R_M$  (**Figure 1d**). The change in resistance is triangular if the rate of change in the memristor resistance does not depend on its value. The rate of change is proportional to the current according to the drift-diffusion model approximation [3].

The input current impacts on the speed of memristor resistance change. The speed is increased at the same signs of the input current and the generator current and it is decreased in opposite case.

## 2.2 Introducing the control of threshold parameters in memristor based oscillator circuits

Standard control approach in memristor based oscillators (MBO) is the exploitation of input signal to control the rate of change in the state of the memristor.

In contrast from this, the main idea of considered controlling approach is to send the input signal not directly to the memristor device but to the comparator circuit and as result to control oscillator circuit behavior by change of interval of memristor resistor variation.

The possible schematic of memristor based oscillator with controlled threshold parameters [50] is given in **Figure 2**. This oscillator element provides the desired functionalities.

The purpose is to change the comparator thresholds using the input voltage  $V_{IN}$  and to control the boundaries of range of memristor resistance variation by input voltage. In this case input voltage  $V_{IN}(t)$ , limited by the region  $V_{OUT}(t) \geq V_{IN}(t) \geq 0$ , shifts the range of  $R(t)$  change:



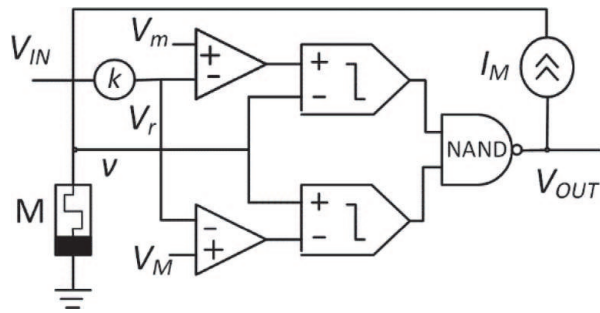


**Figure 2.** Schematic of memristor based oscillator with controlled threshold parameters. The oscillator circuit contains memristor M, two-threshold comparator (TTC), summing elements, attenuator k ( $V_r = kV_{IN}$ ), current source  $I_M$ , logical element NAND.

$$R_m - r(t) \leq R(t) \leq R_M - r(t). \tag{2}$$

Here  $r(t) = V_r(t)/I$  is conditional resistance. In order to avoid exceeding the limits of the range of changes in the memristor resistance, the following inequalities are supported:

$$r(t) < R_m - R_{ON} \text{ and } r(t) < R_{OFF} - R_M \tag{3}$$

The original comparator thresholds  $V_m$  and  $V_M$  are converted into active thresholds in this case.

It can be mentioned that the state of the MBO can be characterized by phase. The phase is determined by the values of two variables:  $R(t)$  and  $\text{sign}(dR/dt)$ .

The fundamental difference between the proposed control approach and the conventional approach is following: the change of the memristor state does not depend on the time of the drive signal arrival under standard control and the state change depends on the time of arrival of the drive signal for proposed approach.

The different character of impact of driving pulses on MBO behavior is shown in **Figure 3**. The input current  $i_{in}$  impacts on the rate of change in the memristor resistance (**Figure 3a**). In this case the speed increases at the same signs of the input

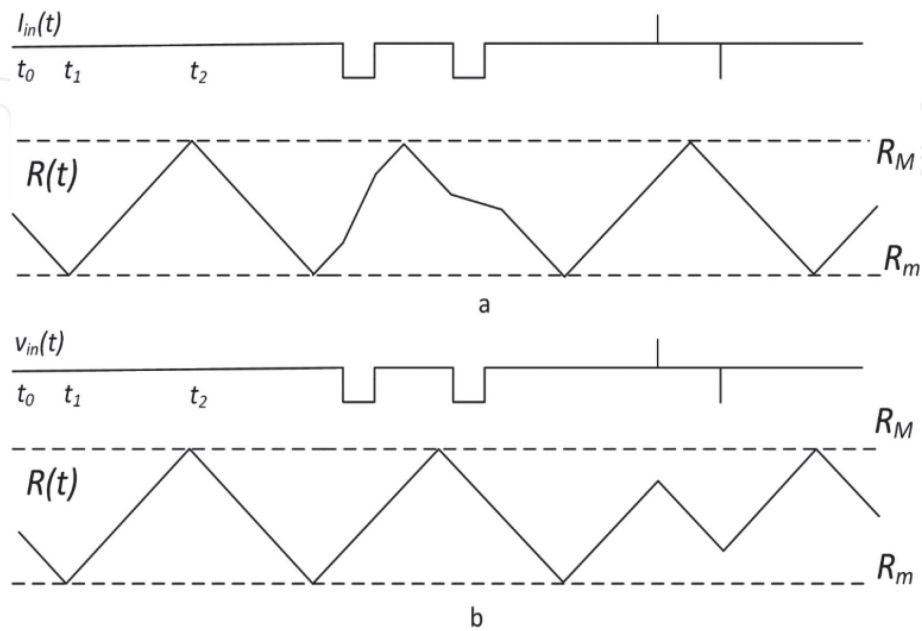


**Figure 3.** The different character of impact of driving pulses on varying memristor resistance  $R(t)$ : (a) excitation by input current  $i_{in}$ , (b). excitation by input voltage  $v_{in}$  to control thresholds.

current and oscillator current and it decreases otherwise. The input voltage  $V_{IN}$  is applied to the comparator to change its thresholds and to determine the range of resistance changes (**Figure 3b**).

The input current signal  $i_{in}$  is integrated. Its effect on the waveforms depends on the duration of the signal and on the phase of the process, in other words on the sign of the resistance change. The long current pulses slow down or accelerate the transient process but short current pulses do not impact on the resistance value.

The input signal  $V_{IN}$  applied to the input of the comparator directly before reaching the threshold can affect the switching process even with a small value of the coefficient  $k$ . At other times the comparator sensitivity to the input signals is reduced. This is illustrated in **Figure 3b**. The long-time pulses applied to the comparator input do not affect the trajectory  $R(t)$ . But even a short positive pulse before reaching the upper threshold resistance  $R_M$  leads to a decrease in the switching threshold and to earlier start of reducing memristor resistance. Similarly, a short negative pulse before reaching the lower threshold resistance  $R_m$  leads to an increase in the lower switching threshold. This leads to beginning of growth of the memristor resistance.

### 2.3 Applicability of memristor based oscillator circuits with control of thresholds in oscillator networks

The pointed out features of two considered approaches to control MBOs predefine their exploitation in oscillator networks. The current inputs are more suitable for controlling the state of network elements by external signals. The voltage inputs with control of thresholds should be used to organize interaction of network elements with each other including synchronization mode of oscillators.

Then we will limit ourselves to the consideration of MBOs with voltage inputs and corresponding control of thresholds. Such an oscillator element can be considered as binary element with the binary input  $v_{in}$  (**Figure 4**).

The current is positive and the memristor resistance decreases at the output signal  $v_{out} = "1"$ , until the resistance reaches the lower threshold  $R_m - r = R_m - kv_{in}/I$ . At output signal "0" ( $v_{out} = "0"$ ) the current through the memristor is negative, its resistance increases until it achieves the upper threshold  $R_M - r = R_M - kv_{in}/I$ .

Thus, input state  $v_{in} = "1"$  slows down the exit from the state  $v_{out} = "1"$ , and accelerates the exit from the state  $v_{out} = "0"$ .

It can be mentioned that considered MBOs with voltage control of thresholds are well suitable for synchronization mode of coupled oscillators due to high sensitivity to external input and fast transient to synchronization steady state.

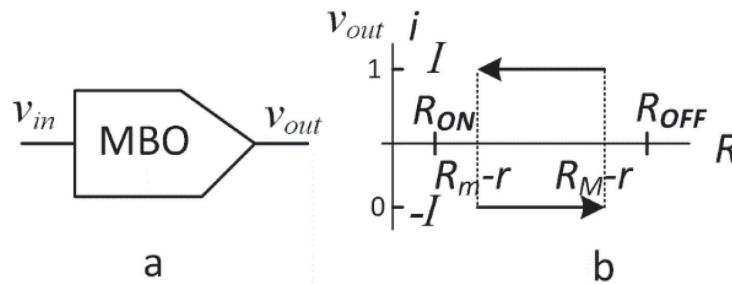


**Figure 4.** Binary MBO element (a) and hysteresis loop for MBO resistor (b) at phase plan taking into account threshold shift.

## 2.4 Model equations

The linear drift model [3] can be applied to describe the behavior of the memristor device. This model involves “instant” voltage–current characteristic for the instantaneous value of resistance

$$v = R \cdot i \quad (4)$$

and control characteristic given by differential equation:

$$\frac{dR}{dt} = -\mu \frac{(R_{OFF} - R_{ON})R_{ON}}{D^2} i = -\gamma i, \quad (5)$$

The model has the following parameters: the high memristor resistor value  $R_{OFF}$ , the low memristor resistor value  $R_{ON}$ , ion mobility  $\mu$ , the semiconductor film thickness  $D$ ,  $\gamma$ -is inertial parameter. These parameters have the following typical values:

$R_{OFF} = 10 \text{ kOhm}$ ,  $R_{ON} = 1 \text{ kOhm}$ ,  $\mu = 10^{-14} \text{ m}^2 \text{ s}^{-1} \text{ V}^{-1}$ ,  $D = 10 \text{ nm}$  [3],  $\gamma = 10^9 \text{ V A}^{-2} \text{ s}^{-1}$ .

The switching time of the memristor device under constant current  $I$  can be estimated as

$$T_R = \frac{R_{OFF} - R_{ON}}{\gamma I} \approx \frac{R_{OFF}}{\gamma I}, \quad (6)$$

This time is 100 ms for current value 100  $\mu\text{A}$ .

To describe the behavior of oscillator with comparator it is convenient to exploit the dimensionless parameters and variables. The dimensionless time is also applied. Such dimensionless variables can be obtained by normalizing. The normalization of resistances is performed using division by  $R_{OFF}$ , respectively for voltages division by  $(I \cdot R_{OFF})$  is applied and for time - division by  $T_R$ . As a result we have  $R_{OFF} = 1$ ,  $R_{ON} = 0.1$  and  $\gamma = 1$ .

Taking into account the threshold shift the comparator model with current generator  $i = i(v)$  (**Figure 1a**) is described by the equations

$$i(v) = \begin{cases} 1, & \text{if } v > V_m - kv_{in} \\ -1, & \text{if } -(V_m - kv_{in}) < v < V_m - kv_{in} \\ 1, & \text{if } -(V_m - kv_{in}) > v \end{cases} \quad (7)$$

Taking into account the binary variables the equations Eqs. (4), (5), and (7) can be transformed to single piecewise constant equation with respect to the variable  $R$

$$\frac{dR(t)}{dt} = \begin{cases} -1, & \text{if } R(t) > R_M - r(t), \\ 1, & \text{if } R(t) < R_m - r(t), \\ \frac{dR(t - \Delta\tau, \Delta\tau \rightarrow 0)}{dt}, & \text{if } R_M - r(t) > R(t) > R_m - r(t), \end{cases} \quad (8)$$

where  $r(t) = kv_{in}(t)/I$  –as mentioned above, variable that reflects the change in the threshold under the influence of external signal. To save the oscillation conditions the following restrictions for  $r(t)$  must be satisfied:

$$R_{OFF} > R_M + r(t), R_M - r(t) > R_m + r(t), R_m - r(t) > R_{ON} \quad (9)$$



The solution of equation Eq. (8) has character of triangular oscillations in the range  $R_m - r < R(t) < R_M - r$ .

## 2.5 Features of reactance-less memristor based oscillators in low frequency applications

The model equation Eq. (5) describes an important feature of memristors - the property of inertia. Due to this property it is possible to construct the reactance-less oscillators or in other words oscillators without inductors and capacitors. In this case the charge and discharge of reactive components in conventional oscillators is replaced by changing the memristor resistance (Eq. (5)). The duration of these processes is determined by the inertial parameter  $\gamma$ . The typical times of switching of the memristor devices are determined by Eq. (6). Thus, typical current value 100  $\mu\text{A}$  corresponds to oscillator frequency 10 Hz.

The prospects of application of such oscillators are associated primarily with the development of low-power low-frequency oscillator circuits for neuromorphic systems and biomedical equipment.

The low-frequency operation range is the main application area of memristor oscillators [21]. Low frequency oscillators are important for many applications but their design is connected with significant difficulties due to the large values of capacitors required for low oscillation frequencies [59]. Since the frequency of operation of conventional RC relaxation oscillators is inversely proportional to the time constant,  $\tau = R \times C$ , low-frequency operation requires high capacitance [21]. In this case the typical capacitance value may exceed 1  $\mu\text{F}$ , capacitor occupies an area of more than  $\text{mm}^2$ . Such an area size contradicts the implementation in integrated circuits. This leads often to off-chip placement of the capacitor [21]. The special-purpose techniques are developed to overcome this problem and to avoid the use of impractically large component values [59, 60]. Thus, relatively novel technique was used to implement the oscillator on-chip, but the capacitor consumed 77.8% of the total chip area [60].

It can be mentioned that the problem is solved automatically with applying reactance-less MBOs due to very small area of memristor devices. For the considered MBO circuits of type (Figure 2) the size of area is determined by the area occupied by CMOS comparator.

## 2.6 Alternative circuitry

In this type of MBO the comparator plays the role of control circuit in switching the direction of the memristor current. It can be noted that this function can be performed by other active circuit elements.

In particular, circuit with a series connected two devices can be considered: memristor and device with negative differential resistance (NDR). This circuit can generate relaxation oscillations when the generation conditions are satisfied.

There is no need for an active load in such circuits. This is advantage of oscillator circuits based on memristor with NDR. In particular, such two-terminal devices can specified by S-shaped I-V characteristics. In this case the memristor itself can have two state given by high and low resistance values [35]. The relaxation oscillations become possible when memristor is connected to a passive two-terminal circuit. Such oscillators can be connected to each other by resistive or resistive-capacitive couplings. This type of oscillators corresponds to circuits with the current input.

Various two-terminal devices can be used as the load in oscillators based on memristors with NDR. Among them, devices with a structure similar to memristors that exploit thin layers of insulators are promising. Creation of such devices based

on silicon oxides [36, 61] seems to be the most promising now. New emerging memristive technologies such as SiO<sub>x</sub>-based memristors are discussed in [61]. The compatibility with standard CMOS technology provides a good perspective for the implementation of hybrid CMOS-memristive designs in various applications.

Recent results [61] demonstrate advantages of the architecture of memory cell comprising memristor and selector. It is expected that under certain conditions such an emerging device architecture can act as an oscillator.

In the following text the consideration is limited by oscillator circuits based on memristor devices [3], although the results presented below for coupled oscillator elements can be extended to above mentioned circuit architecture.

### 3. Behavior of coupled memristor based oscillators with positive couplings

#### 3.1 Operating principles

The analysis of behavior of two coupled identical MBO with positive connection is presented below.

This circuit is shown in **Figure 5**. It contains MBO1, MBO2, an adder at the input and a phase detector at the output [50]. To provide an external control the excitation signal  $V_C$  is transmitted using an adder at the input. The phase detector at the output is used to identify the synchronization mode of coupled oscillators. If there is no synchronization between the oscillator stages MBO1 and MBO2 then output signal  $V_s = 1$  and  $V_s = 0$  if there is synchronization.

The coupling strengths between the MBOs specified by coefficient  $k$  impact on the behavior of this system significantly.

The rates of change of memristor resistances  $R_1$  and  $R_2$  are equal in modulus for identical MBOs. But these rates may differ in signs. By such a way the variables  $R_1$  and  $R_2$  and the signs of derivatives  $dR_1/dt$  and  $dR_2/dt$  can be considered as system states and may specify the behavior of system of two coupled oscillators.

The phase plane with axes  $R_1$  and  $R_2$  (**Figure 6**) can be exploited for analysis of different behavior versions of such a system. The analysis is based on model Eq. (8). In this case, the trajectories of moving the image points are straight lines. They pass at angles of  $\pm \pi/4$  on phase plane. Four trajectories can pass through each point of phase plane. The sign of  $dR/dt$  defines one from them.

The boundaries of the area of trajectories movement are specified by the threshold resistances. When the trajectory reaches the boundary the sign of the derivative  $dR/dt$  changes and trajectory is mirrored from the boundary. The boundaries can shift themselves at this time point.

If the external excitations are absent then the threshold of each MBO depends on positive pulse from the neighboring MBO. In particular the lower limit of the resistance of each MBO is reduced to  $R_m - r$ . As a result the area of the allowable system states on the phase plane in self-oscillating mode is determined by the square with vertices  $(R_M, R_M)$  and  $(R_m - r, R_m - r)$  (**Figure 6**). The area of

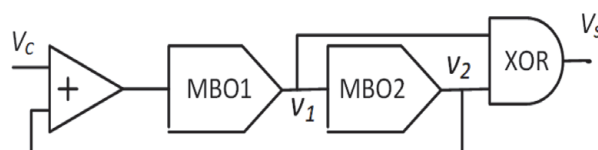


**Figure 5.**  
 Schematic of coupled memristor based oscillators (MBOs).

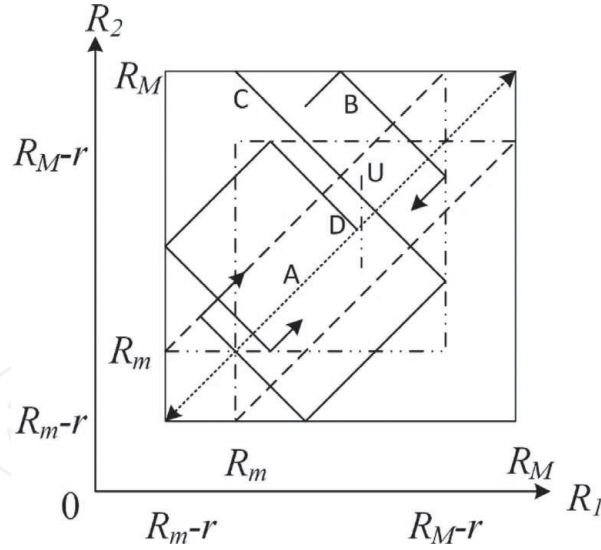


**Figure 6.**

The boundaries and trajectories at phase plane of changing the variables  $R_1$  and  $R_2$  for coupled MBOs: solid lines – boundaries for case  $dR_1/dt = dR_2/dt$ , dash-dotted lines – boundaries for case  $dR_1/dt \neq dR_2/dt$ , solid lines with arrows – the trajectories of  $R_1$  and  $R_2$  with different initial conditions. The areas of stable trajectories are limited by dashed lines.

stationary trajectories is located insight this square. This area is limited by the dashed lines in **Figure 6**.

For the existence of a stationary trajectory, the following necessary and sufficient conditions must be met: the image points must be located in the area indicated above, and the signs of the derivatives must be identical.

If the variables are located at the main diagonal in this area and the specified conditions are met, then the variables reach the threshold simultaneously (dotted line A in **Figure 6**). Their moving directions also change simultaneously. They continue to move along the main diagonal. When the threshold line is reached by one variable on the other lines parallel to the main diagonal in this area, the sign of its derivative changes. This is followed by the threshold change for another variable with a corresponding change in the sign of its derivative. The trajectory is saved, but the movement along it occurs in the opposite direction. Note that the phases of the oscillations of the resistors are the same ( $V_s = 0$ ) for stable trajectories.

If the starting points of trajectories are located outside area of stationary trajectories (**Figure 6**) then such trajectories are reflected after reaching the boundaries. If in this case the signs of the derivatives are the same then the segments of the trajectories tend to the stability region. The reflection character is defined by the boundaries with different signs of derivatives  $dR_1/dt \neq dR_2/dt$  (dashed lines in **Figure 6**). Any trajectory ends in the region of stable trajectories in result. Such behavior is illustrated in **Figure 6** by examples of the trajectories B and C. It can be seen that the trajectory B falls into the stability region after two reflections and the trajectory C - after four reflections.

The considered circuit with two coupled identical oscillator elements (**Figure 5**) has a set of stable and unstable steady state trajectories. The difference between the maximal values of the variables  $R_s = R_{1max} - R_{2max}$  can be exploited as characteristic of stable steady state trajectories. It can be mentioned that zero value  $R_s$  ( $R_s = 0$ ) corresponds to the main diagonal on phase plan (**Figure 6**). This characteristic reaches the value  $R_s = \pm r$  at the boundaries of the stable region. The each stationary trajectory (each value of  $R_s$ ) corresponds to a certain period of triangular oscillations which equals to

$$T_s = 2 \frac{R_M - R_m + r - R_s}{\gamma I}. \quad (10)$$

Let duration of the additional external control signal  $V_C$  be shorter than period  $T_S$ . This signal  $V_C$  can change the boundary and the trajectory of movement on the phase plane respectively. **Figure 6** shows the boundary  $U$  created by an external signal. The trajectory  $D$  in **Figure 6** illustrates the transition to new stable trajectory under the influence of an external signal. The starting point of trajectory  $D$  is located at the main diagonal. The trajectory  $D$  moves away from the main diagonal under the external excitation. After three reflections (**Figure 6**) the transition of image point to new stable trajectory is carried out.

### 3.2 Features

It can be mentioned that for considered coupled MBOs the movement along the trajectory in the direction opposite to the original one can be provided by changing the signs of the derivatives. This property can be called as reversibility of trajectories. The property is valid for stable trajectories as well as for any unstable trajectories before its transition to stable ones. Such a feature may be foundation for the management of coupled MBOs.

In order to get from the original fixed trajectory (for example A) onto given trajectory (for example D), it is enough to choose the intersection point of the predetermined path with the threshold line ( $R_2 = R_m$ ) and then to construct the trajectory of leaving it until the inevitable intersection with the original trajectory using change in derivative sign. The control signal with short duration and sufficient amplitude moves the image point to the specified trajectory.

The process of transition to stationary trajectory can be represented using the mapping function of the value  $R_S$  over the period:  $R_S(n+1) = P(R_S(n))$  (**Figure 7**). The value of  $R_S$  for the  $n$ -th period is given in **Figure 7** at the abscissa axis and similar value as a result of Poincare mapping for  $n+1$  period is shown at the ordinate axis. The area of stable states belonging to the diagonal D (**Figure 7**) satisfies the condition:  $-r < R_S < r$ , that corresponds to the area of stationary trajectories.

Until  $|R_S| > 3r$  the return of  $R_S$  to the region of stable states is performed with stepsize equal to  $4r$ . If  $R_S$  located in the interval  $r < R_S < 3r$  then the return occurs in one step equal to  $2(|R_S| - 1)$ .

As follows from this analysis, the speed of the transition process from the excited state to the stationary state depends on the coupling strength or in other words on the coefficient  $r$ . The width of the stability area also depends on coupling strength. The return to the stationary trajectory after external excitation can be relatively long at low values of factor  $r$ . It can be expected that the return time is

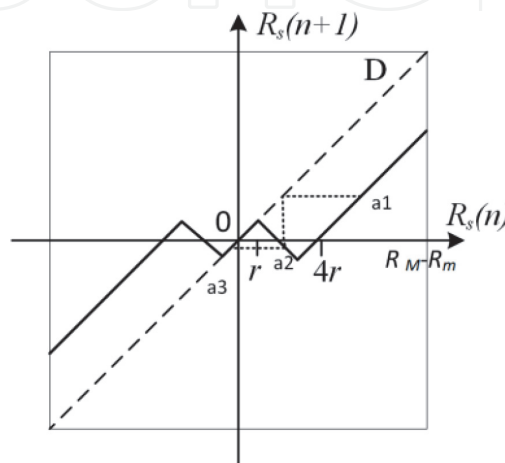


**Figure 7.**  
 The function of mapping the difference in the states of the coupled MBOs for period.



proportional to the amplitude of the external signal in a certain range of amplitude varying.

The situation changes significantly when the excitation has a long duration, comparable to or exceeding the duration of the period  $T_S$ . In this case new values of the threshold resistances for  $R_1$  are set during the action of the input signal. Then the value  $R_1$  will change within this interval of variation. The duration of the transition to the perturbed state will also depend on the coupling strength. The output signal will appear on the phase detector in this case. The return to the stationary trajectory will repeat again after completion of the input signal and signals at the output of the phase detector will appear again.

The behavior of self-oscillating coupled MBO is described by piecewise-constant differential equations. As a result, the complete analytical solution can be obtained. In practice, it reduces to solving the problem of elastic reflection of a point inside a rectangle with edges positioned depending on the sign of the point's speed.

### 3.3 Simulation examples

Below the results of simulation of the coupled MBOs are given. The simulation examples demonstrate the opportunity to control the state of the coupling MBOs and illustrate also waveforms of generation of the pulse trains at the input excitation.

The time is defined as dimensionless variable. Also, the dimensionless values of the circuit parameters and variables were used during simulation. Among them:  $R_M = 0.8$ ,  $R_m = 0.4$ ,  $r = 0.1$ .

#### 3.3.1 Example 1: managing the state of coupling MBOs

The considered circuit example has a set of stable and unstable steady-state trajectories and provides complex transformation of input signal. The simulation example illustrates the presence of three stable steady-state periodic solutions (**Figure 8**) correspond to  $R_s = R_{1max} - R_{2max} > 0$ ,  $R_s = R_{1max} - R_{2max} < 0$ ,  $R_s = R_{1max} - R_{2max} = 0$ .

Input signals lead to switching of stable trajectories and provides various modes in application.

Let the starting points for the variable resistances be the same al for MBO1 and MBO2 ( $R_1(0) = R_2(0) = 0.5$ ). When the first control pulse with amplitude  $V_C = 0.4$  and duration  $T = 0.5$  is applied to MBO1 the process is generated in which the amplitude of the resistance oscillations of MBO1 is greater than the similar amplitude for MBO2. The state corresponds to inequality  $R_s > 0$  (**Figure 8**). The second

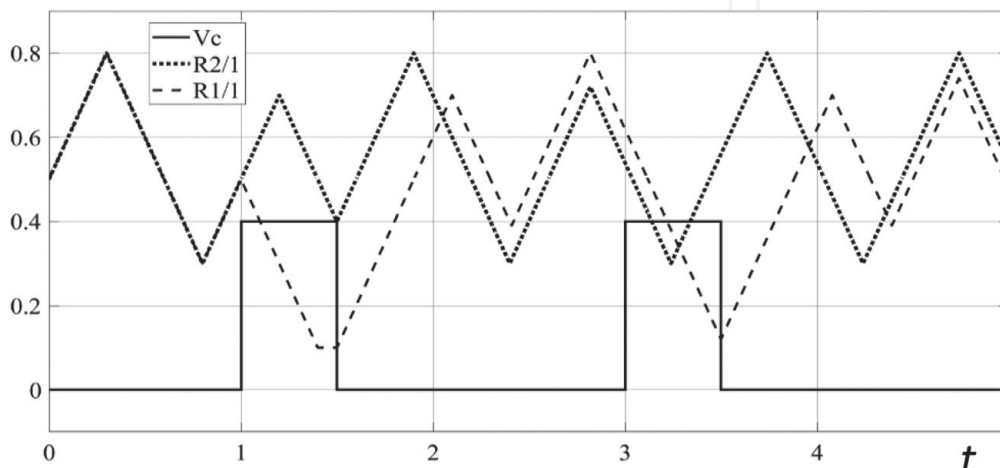


**Figure 8.**

The computed waveforms in the coupled MBOs.  $V_C$  - the solid line,  $R_1(t)$  - dashed line,  $R_2(t)$  - dotted line.



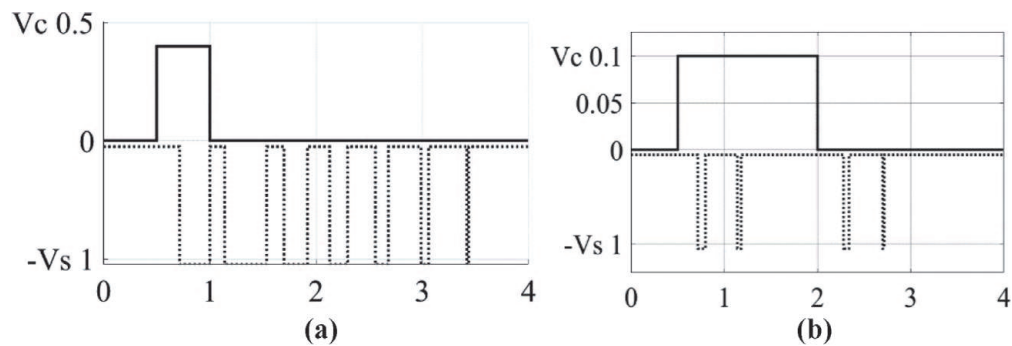


**Figure 9.**  
 Generation of train of output pulses (dotted line) under the action of the input signal of short duration (a) and long duration (b).

control pulse leads to change of trajectory and generates the steady state corresponding to inequality  $R_S < 0$  (**Figure 8**).

By such a way this simulation example confirms the predicted change of memristor states in the considered circuit under control pulse excitation.

### 3.3.2 Example 2: generation of pulse train by coupling MBO under the action of the input signal

Let the initial setting conditions for MBO1 and MBO2 be the same that corresponds to the zero voltage  $V_S$  at the output of the detector (**Figure 9a**). After the input signal with amplitude  $V_C = 0.5$  and duration  $T = 0.5$  (**Figure 9a**) their synchronization is violated for time proportional to the amplitude of the input action. The output signal of the comparator with amplitude  $V_S = 1$  appears after the beginning of the transition to the perturbed trajectory and pulses remain for a long time.

When long-term input signal  $T=1.5$  of relatively small amplitude  $V_C = 0.1$  is applied the transition to the perturbed trajectory and exit from it is performed in shorter time (**Figure 9b**). The output signal  $V_S = 1$  occurs both after the rising slope and after the fall slope of the input pulse.

## 3.4 Output

The coupled memristor based oscillators with positive couplings have a set of stationary states in self-excitation mode.

An external signal can initiate a transition from one stationary state to another. Also such a signal can remove the system from the region of stationary states to the excited mode. This excitation is saved after completion of the input signal. The transition to new steady state takes some time after completion of the external excitation. The pulse train is generated at the comparator output during this time interval.

The coupling memristor based oscillators can be considered as the analog-to-digital converters that provide conversion of input amplitude variation.

## 4. Behavior of coupled memristor based oscillators with inverting connections

### 4.1 Operating principles

The connection types of the coupled memristor based oscillators (MBO) and the values of the coupling strengths between them impact significantly on the character of their behavior.

The schematic of coupled MBOs with inverting connections and binary output signals is shown in **Figure 10**. The circuit of this oscillator element contains [49] two identical oscillators MBO1 and MBO2. If the direct signal  $V_1$  applied to input MBO2 then MBO1 receives an inverted signal ( $-V_2$ ) from MBO2 output. The circuit contains also output phase detector  $F(V_1, V_2)$  and input adder. The phase detector performs logical function over the binary outputs MBO1 and MBO2. The input adder provides the receipt of both the control analog signal  $V_C$  and the inverted signal ( $-V_2$ ) at MBO1 input.

The state of the considered oscillator system can be specified by the variables  $R_1$  and  $R_2$  and time derivatives  $dR_1/dt$  and  $dR_2/dt$ . The modules of the rates of change of memristor resistances  $R_1$  and  $R_2$  are the same for identical MBOs but signs of these rates may differ.

The detailed analysis of behavior of this system using phase plane for variables  $R_1$  and  $R_2$  is given in [49]. The feature of phase portrait for coupled MBOs with inverting connections is related with the derivatives of variables  $R_1$  and  $R_2$  that take the values  $\pm 1$ . Due to this feature the trajectories of the image point are inclined straight lines with angle of  $\pm \pi/4$  relative to the coordinate axes.

The ratio of coupling coefficients with opposite signs  $r_1 = -k_1 V_2(t)/I$  and  $r_2 = k_2 V_1(t)/I$  significantly affects character of behavior. The cases of equal values ( $|r_1| = |r_2|$ ) and different values ( $|r_1| \neq |r_2|$ ) are discussed in [49].

Introducing the additional notations  $r$  and  $r_M$  two possible versions can be considered for different values of coupling coefficients:  $|r_1| = r_m < r = r_2$ ,  $|r_1| = r_M > r = r_2$ . First case with the dominance of direct positive coupling corresponds to antiphase oscillations and second case with dominance of inverting negative coupling corresponds to in-phase oscillations.

The period of antiphase oscillations equals to  $T = 2 (R_M - R_m - r_m)/\gamma I$  and the period of in-phase oscillations is  $T = 2 (R_M - R_m - r)/\gamma I$ .

The external control signal impacts on the phase trajectory of the system. Consider then the case with  $|r_1| = r_m$ .

The range of varying MBO1 threshold voltage is shifted due to applying the control signal  $V_C$ . The additional shift in the threshold resistances  $r_C = V_C/I$  is generated by control signal  $V_C$ . Due to action of the  $V_C$  signal the following active restrictions determine the interval of varying memristor resistances of MBO1 and MBO2 circuits.

$$R_m + r - r_C \leq R_1(t) \leq R_M + r - r_C \text{ at } dR_2/dt < 0 \quad (11)$$

$$R_m - r_C \leq R_1(t) \leq R_M - r_C \text{ at } dR_2/dt > 0 \quad (12)$$

$$R_m - r \leq R_2(t) \leq R_M - r \text{ at } dR_1/dt < 0 \quad (13)$$

$$R_m \leq R_2(t) \leq R_M \text{ at } dR_1/dt > 0 \quad (14)$$

**Figure 11** illustrates such shift at the phase portrait of the system with control signal. As follows from formulas Eqs. (11) and (12), the threshold resistances for  $R_1$  are decreased (**Figure 11**) but the threshold resistances for  $R_2$  remained unchanged.

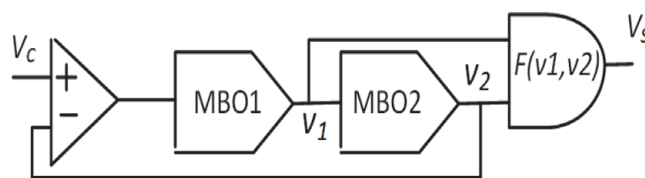


**Figure 10.**  
The system of coupled MBOs with inverting connections.

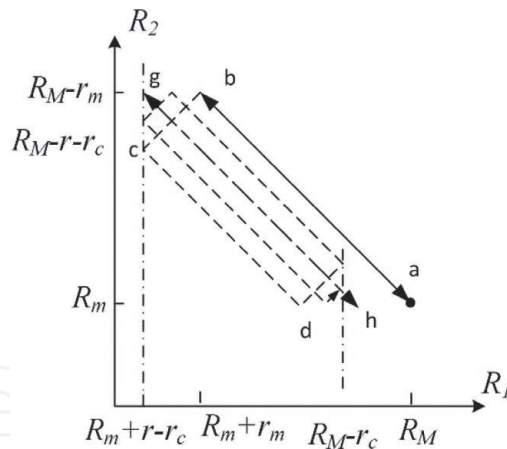


**Figure 11.**  
 Phase plane of system of coupled MBOs with inverting connections under external excitation.

For this reason, the parallel shift of trajectories at the phase portrait (**Figure 11**) corresponds to impact of external control signal.

Let the initial stable trajectory of the system before an external excitation correspond to line segment (*ab*) and after an external excitation the displaced trajectory corresponds to line segment (*gh*). When a constant control signal is applied for sufficiently long time, the transition to the trajectory (*gh*) is inevitable. It is caused by change in the sign of  $dR_2/dt$  and reducing the threshold resistance to  $R_m + r - r_c$  when the point *b* reaches the border at  $R_1(t) = R_m + r_m$ . **Figure 11** illustrates the movement of image point from *b* to *c*, then to *d*, until it falls on the trajectory (*gh*).

The difference  $\Delta = r_2 - |r_1|$  determines the width of the stability area and impacts on the speed of the transition process to new trajectory. It should be expected that due to the piecewise linear character of transients the return time will be proportional to the input amplitude in certain range of amplitude variation of control signal.

## 4.2 Simulation example

The results of the behavior simulation of the coupled MBOs with inverting connections are given below for case of short input signal.

The computed waveforms for the oscillator system with phase detector NOR are shown in **Figure 12**. In this case stable antiphase oscillations are observed in the system under the absence of an external signal.

The following values of coupling factors were selected:  $r_2 = 0.1$ ,  $r_m = 0.09$ . These values of coupling factors mean that positive coupling in connected MBOs is stronger than negative coupling. The dimensionless parameters and variables are used below and the dimensionless time is also applied.

Let a starting point of system state be the stable trajectory with antiphase oscillations. The initial values of resistances  $R_M = 0.8$ ,  $R_m = 0.4$  are selected. The output signal  $V_S = 0$  corresponds to the stable trajectories of initial state (**Figure 12**). The positive pulse with amplitude of 0.05 and duration of 0.1 arrives at time  $t = 0.9$ . It causes the delay of switching of MBO1. The series of four output pulses is generated (**Figure 12**) while the system is in an excited state and the antiphase is violated.

The difference  $\Delta$  in the coupling factors significantly impacts on the speed of transition to a stable trajectory. If this value is small the transient process can be

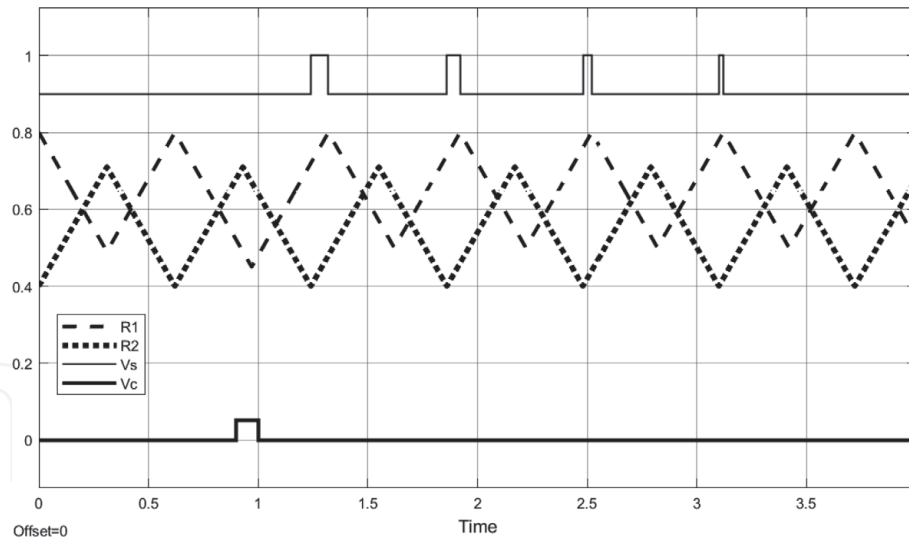


**Figure 12.**

*Example of simulating the timing diagram of the generation of output pulse series in the coupled MBOs with inverting connections.*

significantly delayed. At fixed values of the coupling strengths the input amplitude and time of arrival of the input pulse determine the time of transition to a stable trajectory. Due to this property the conversion of the input amplitude to the duration of the transition process can be performed.

### 4.3 Output

The system of two coupled MBOs with the inverting connection can be characterized by the following capabilities:

1. antiphase or in-phase steady state oscillations are generated depending on relation of coupling strengths;
2. the control signal causes transition to new stable state if the pulse amplitude is sufficient to change the threshold values;
3. appearance of pulses at the detector output is associated with the transition to new state and violation of the synchronization of oscillations;
4. the duration of the transient process and the number of pulses at the detector output are proportional to the amplitude of the drive signal and they are inversely proportional to the modulus of the difference in the coupling coefficients.

## 5. Properties of coupled memristor based oscillators for use in binary oscillator networks

The coupled MBOs have useful functional qualities for a number of applications. The possible application of connected MBOs as the basic elements of binary oscillation networks (BON) is discussed below. In particular, the BON with ring architecture and star-like architecture are considered. The presented before coupled MBOs with positive couplings and coupled MBOs with inverting connections are used for this purpose.

## 5.1 Features of binary oscillator networks based on memristor oscillators

The important properties of coupled MBOs are the simplicity of external managing the conditions of the oscillator injection locking, as well as fast frequency capture under relatively small impact amplitude.

The external excitation can violate the synchronicity of the coupled MBOs. The time to restore synchronization depends on the amplitude of the external impact and coupling strengths between the MBOs. As a result, the coupled MBOs provide the modulation of pulse trains desired for the implementation of oscillatory artificial neurons (AN).

By such a way, it becomes possible to apply the simpler coupling systems of the first order instead of using high-order nonlinear systems with reactive circuit elements and with high requirements for the element parameters.

Note that coupled MBOs belong to the class of binary oscillator and can be exploited in BON on base of integrated technologies. Using binary oscillators with binary output signals [46–48] is one of the promising lines for constructing oscillatory neural networks that are most suitable for integrated technologies. In such binary oscillator networks information is represented by binary streams.

The connection of  $N$  MBOs is described by system of  $N$  equations for variables  $R_i(t) (i = 1, 2, \dots, N)$ . This system has the view of type Eq. (8):

$$\frac{dR_i(t)}{dt} = \begin{cases} -1, & \text{if } R_i(t) > R_M - r_i(t), \\ 1, & \text{if } R_i(t) < R_m - r_i(t), \\ \frac{dR_i(t - \Delta\tau, \Delta\tau \rightarrow 0)}{dt}, & \text{if } R_M - r_i(t) > R_i(t) > R_m - r_i(t), \end{cases} \quad (15)$$

The outputs of the transmitting MBOs are connected to the inputs of the receiving MBOs directly or via logic gates. Therefore the variables  $r_i(t)$  are binary functions of the outputs of the transmitting MBOs:

$$r_i(t) = k_i \cdot F_i(v_{out1}, v_{out2}, \dots, v_{outN}) \quad (16)$$

where  $F_i(\dots)$  is a logical function of  $N$  binary variables (0, 1). In this case the relationship between binary variable  $v_{out}$  and  $dR/dt$  is unambiguous.

The system of equations Eqs. (15) and (16) describes behavior of BON in autonomous mode. If there are external binary signals, they should be included into the  $F_i$  functions as additional external variables.

As simple examples of the elements of the binary oscillator networks based on memristor oscillators we can point out ring structure (**Figure 13**) which can be considered as extension of the considered before two coupled identical MBO with positive couplings (**Figure 5**) and also star-like structure (**Figure 14**) with applying the coupled MBO with possible inverting connections.

## 5.2 Some simulation results

Some simulation results to confirm the features of BON based on MBOs are presented below. To simulate the versions of BON fragments the dimensionless parameters of the variables were used:  $R_M = 0.8$ ,  $R_m = 0.4$ .

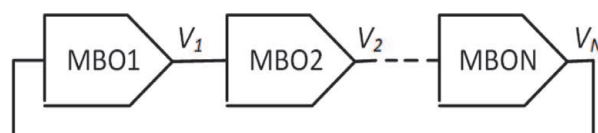


**Figure 13.**  
 Example of BON ring structure using memristor based oscillators.



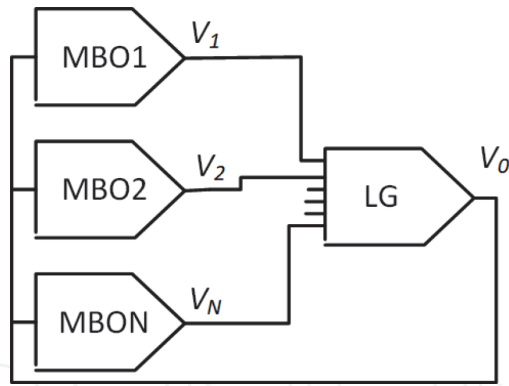


**Figure 14.**  
*Example of BON star-like structure using memristor based oscillators.*

The circuit element of star-like structure containing two coupled MBOs was selected for simulation. This circuit contains also logical element OR. The coupling strength has the value  $r = 0.05$ .

The computed waveforms are given in **Figure 15**. The transient process from starting point to steady state is shown. The oscillators MBO1 and MBO2 have the different initial states:  $R_1(0) = 0.4, R_2(0) = 0.8$ . Then the oscillators tend to periodic steady state  $R_1(t) = R_2(t)$  and reach it during four periods. The outputs of MBO1 and MBO2 are identical in steady state mode. This state corresponds to logical “0” due to applying the logical function XOR. The change of logical function XOR is shown in the lower curve in **Figure 15**. In this case the pulses of logical “1” appear under misalignment of the MBO1 and MBO2 outputs.

It can be mentioned that variation of initial state for MBO2 oscillator leads to change in duration of the process of steady state establishing (**Figure 15**). So for  $R_2(0) = 0.7, 0.6, 0.5$  the transition to periodical steady state is performed for 3, 2 and 1 periods, respectively. In these cases, the difference in the initial states is a multiple of twice the coupling strength factor (here  $r = 0.05$ ). This case corresponds to the complete synchronization of the oscillations (the phase shift is 0).

In connection with this non-multiple case is of interest. Then the initial states  $R_1(0) = 0.43, R_2(0) = 0.8$  are chosen as examples. The corresponding computed waveforms are given in **Figure 16** for different versions.

As can be seen from **Figure 16a** the oscillations in MBO1 and MBO2 are synchronized with the shift at inverting absence. Steady state is reached for time interval of four periods, the periodic pulses are generated at the output, the phase detector XOR generates short mismatch pulses.

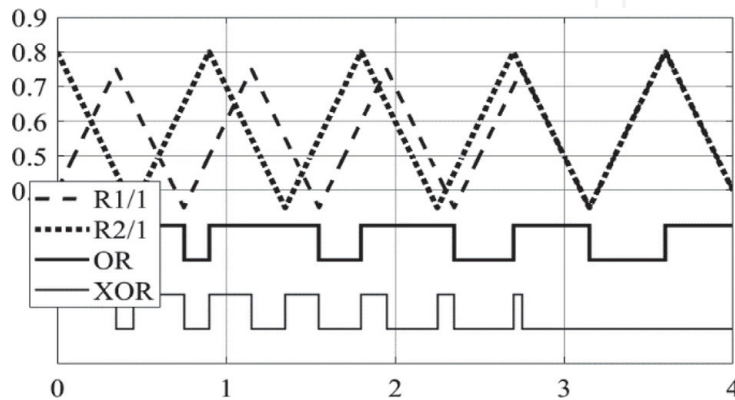


**Figure 15.**  
*The computed waveforms of the transient process from starting point to steady state for coupled MBOs: MBO1- dashed line, MBO2 – dotted line, OR function -solid bold line, function XOR – solid line.*

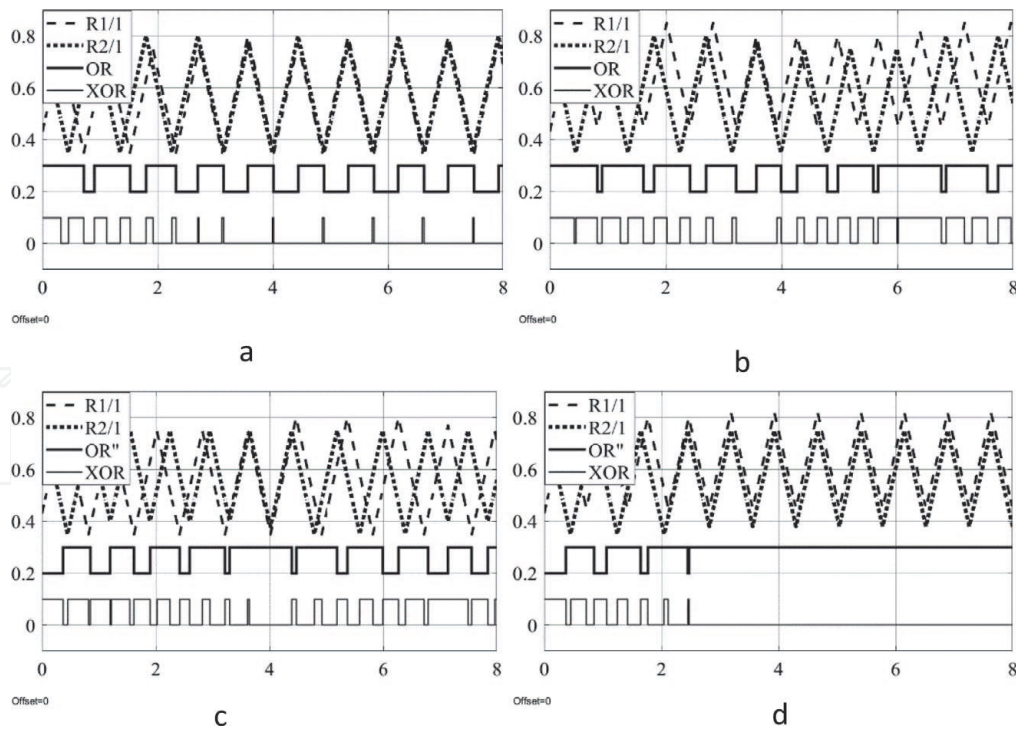


**Figure 16.**  
 The computed waveforms of the transient process for coupled MBOs with the initial states  $R_1(0) = 0.43$ ,  $R_2(0) = 0.8$ . The graphs correspond to the following versions of coupling types: (a) couplings without inverting; (b) couplings with analog inverting MBO1 input; (c) couplings with inverting of the MBO2 binary output; (d) couplings with joint inverting of both types.

The timing diagram of MBOs behavior gets more complicated for cases with inverting the coupling signals (**Figure 16b**). The dependences of  $R(t)$  can be considered as modulated by triangular oscillations. The output signals of the logical element and the phase detector are converted into complex binary sequences with large period. The similar character of waveforms can be observed in the case of logical inversion (**Figure 16c**) when the logical OR circuit receives at the input the inverted signal from the output of MBO2. By such a way if the difference in the initial states is a non-multiple of twice the coupling strength factor then timing diagram of MBOs behavior is complicated for both types of inversion. It is interesting also that the simultaneous use of both types of inversion leads to another character of waveforms (**Figure 16d**). The full synchronization can be achieved after the transient process.

The presented simulation results illustrate the capabilities of coupled MBOs in its application as elements of Binary Oscillator Networks.

## 6. Conclusion

The chapter describes the behavior and application capabilities of the coupled reactance-less memristor based oscillators. This type of coupling memristor oscillators provides the generation of desired pulse trains with the complicate character of behavior. The chapter idea is to apply the simpler coupling systems of the first order instead of using high-order nonlinear systems with reactive circuit elements and with high requirements for the element parameters.

The coupled memristor-based reactance-less oscillators have the set of modes that is enough to provide the complex behavior desired in many applications.

To construct the memristor oscillator circuits the principle of controlling threshold parameters is applied. The constructing the piecewise constant memristor oscillators is one of advantages of this approach.

Two types of oscillator couplings are analyzed in chapter: coupled memristor based oscillators with positive couplings, coupled memristor based oscillators with inverting connections.

The coupling memristor based oscillators can be considered as the analog-to-digital converters that provide transform of amplitude variation. The properties of coupled reactance-less memristor based oscillators open up the possibility of constructing binary oscillator networks on its base for solving a wide range of problems. In particular, star-like binary oscillation networks based on coupled memristor oscillators with only one logical elements create a number of promising applications, including oscillator reservoir calculations, stochastic oscillators, neural networks with probabilistic coding.

## **Acknowledgements**

The reported study was funded by RFBR, project number 19-29-03012.

## **Conflict of interest**


The authors declare no conflict of interest.

## **Author details**

Vladimir V. Rakitin and Sergey G. Rusakov\*  
Institute for Design Problems in Microelectronics of Russian Academy of Sciences (IPPM RAS), Moscow, Russia

\*Address all correspondence to: [rusakov@ippm.ru](mailto:rusakov@ippm.ru)

## **IntechOpen**

© 2021 The Author(s). Licensee IntechOpen. This chapter is distributed under the terms of the Creative Commons Attribution License (<http://creativecommons.org/licenses/by/3.0>), which permits unrestricted use, distribution, and reproduction in any medium, provided the original work is properly cited. 

## References

- [1] Chua L.O., Memristor-missing circuit element. *IEEE Trans. Circuit Theory*. 1971, V. 18, N. 9, pp. 507–519.
- [2] Chua L.O., Sirakoulis G. Ch. A. Adamatzky A., editors. *Handbook of Memristor Networks*. 2019. 1368 p. [https://doi.org/10.1007/978-3-319-76375-0\\_1](https://doi.org/10.1007/978-3-319-76375-0_1)
- [3] Strukov DB, Snider GS, Stewart DR, Williams RS. The missing memristor found. *Nature*. 2008;453(7191):80-83
- [4] Schuman C., Potok T., Patton R., Birdwell J., Dean M., Rose G., Plank J. A Survey of Neuromorphic Computing and Neural Networks in Hardware. *arXiv:1705.06963*. 2017. V1, 19.
- [5] Islam R., Li H., Chen P., Wan W., Chen H., Gao B, Wu H., Yu S., Saraswat K., Wong H. Device and Materials Requirements for Neuromorphic Computing. *Journal of Physics D: Applied Physics*. 2019. V.52. N.11.
- [6] Hopfield J.J. Neural networks and physical systems with emergent collective computational abilities. *Proc. Natl. Acad. Sci. USA*. 1982. 79(8). pp.2554–2558.
- [7] Tamas R, Chua L.O. The CNN universal machine: an analogic array computer. *IEEE Transactions on Circuits and Systems II: Analog and Digital Signal Processing*. 1993. V. 40, N. 3. pp.163-173.
- [8] Izhikevich E. M. *Dynamical systems in neuroscience*. MIT press. 2007.
- [9] James A., editor. *Memristor and Memristive Neural Networks*, IntechOpen, 2018. 324 p DOI:10.5772/66539
- [10] Itoh M., Chua L.O. Memristor Oscillators. *Int. J. Bifurcation Chaos*. 2008. V. 18. N. 11. pp. 3183–3206.
- [11] Talukdar A., Radwan A., Salama K. Generalized Model for Memristor Based Wien Family Oscillators. *Microelectronics Journal*. 2011. V. 42. N. 9. pp. 1032–1038.
- [12] Talukdar A., Radwan A., Salama K. Non Linear Dynamics of Memristor Based 3 Order Oscillatory System. *Microelectronics journal*. 2012. V 43. N.3.pp. 169–175.
- [13] Wang Y., Liao X. Stability analysis of multimode oscillations in three coupled memristor-based circuits. *AE ËÜ -International Journal of Electronics and Communications*. 2016. V.70, N. 12, pp. 1569–1579.
- [14] Banchuin R. On the fractional domain generalization of memristive parametric oscillators. *Cogent Engineering*. 2019. 6:1, 1617094, DOI: 10.1080/23311916.2019.1617094
- [15] Elsonbaty A., Abdelkhalek A., Elsaid A. Dynamical behaviors of coupled memristor-based oscillators with identical and different nonlinearities. *Mathematical Problems in Engineering*. 2018. pp.1-19.
- [16] Forti M., Corinto F. Complex Dynamics in Arrays of Memristor Oscillators via the Flux-Charge Method. *IEEE Transactions on Circuits and Systems I: Regular Papers*. 2017.V.66. N.11. pp.1-11.
- [17] Ponce E., Ros J., Freire E., Amador A. Unravelling the dynamical richness of 3D canonical memristor oscillators. *Microelectronic Engineering*. 2017. pp.1-22.
- [18] Saha, D.C., Saha, P., Ray, A., Roychowdhury, A., On the Synchronization of Synaptically Coupled Nonlinear Oscillators: Theory and Experiment. *Annual Review of Chaos Theory, Bifurcations and Dynamical Systems*. 2016. V.6. pp.1-29.



- [19] Fouda M., Radwan A. Memristor-based voltage-controlled relaxation oscillators. *Int. J. Circ. Theor. Appl.* 2013. V. 42, N. 10, pp.1092-1102.
- [20] Zidan M., Omran H., Smith C., Radwan A. Salama K. A Family of Memristor Based Reactance-Less Oscillators. *Int. J. Circuit Theory and Applications*. 2013. V. 42. № 11. pp. 1103–1122.
- [21] Kyriakides E, Georgiou J. A compact, low-frequency, memristor-based oscillator. *Int. J. Circ. Theor. Appl.* 2015. V.43 pp.1801-1806.
- [22] Radwan A., Fouda M. On the Mathematical Modeling of Memristor, Memcapacitor, and Meminductor. Cham: Springer International Publishing. Switzerland. 2015.
- [23] Khatib M., Mosad, A., Fouda, M., Radwan, A. Generalized Analysis of Symmetric and Asymmetric Memristive Two-Gate Relaxation Oscillators. *IEEE Trans. Circuits Syst. I*, 2013. V. 60. N. 10. pp. 2701-2708.
- [24] El-Naggar A., Fouda M., Madian A., Radwan A. Reactance-less RM relaxation oscillator using exponential memristor model. 2016. 28th International Conference on Microelectronics (ICM). Giza, pp. 361-364, doi: 10.1109/ICM.2016.7847890.
- [25] Rakitin V., Rusakov S. The Signal Converter Based on Monostable Memristor Oscillator. *Problemi Razrabotki Perspektivnih Mikro- i Nanoelektronnih system (MES)*. 2017 (1). pp. 29-32
- [26] Rakitin V., Rusakov S. Operating principles of reactance-less memristor-based oscillators. *Journal of Communications Technology and Electronics*. 2017. V. 62, N.6, pp.621–625.
- [27] Rakitin V., Rusakov S. Principles of the Functioning of Nonreactive Double Memristor Oscillators. *Journal of Communications Technology and Electronics*. 2019. V.64, N.6, pp.622–628.
- [28] Rakitin V., Rusakov S. The Reactance-Less Two-Memristor based Oscillator for Signal Processing. In: 2020 Moscow Workshop on Electronic and Networking Technologies (MWENT). 2020. pp.1-5.
- [29] Mazumder P., Yilmaz Y., Ebong I., Lee W. Memristor-based Cellular Nonlinear/Neural Network: Design, Analysis and Applications. *Neuromorphic Circuits for Nanoscale Devices*. 2018. pp.275-302.
- [30] Mazumder P., Yilmaz Y., Ebong I., Lee, W. Dynamic Analysis of Memristor-based Neural Network and its Application. *Neuromorphic Circuits for Nanoscale Devices*. 2018. pp.303-350.
- [31] Xu B., Lin H., Wang G. Hidden. Multistability in a Memristor-Based Cellular Neural Network. *Advances in Mathematical Physics*. 2020 V.2020, no.9708649, pp.1-10.
- [32] Majdabadi M. Shamsi J., Shokouhi S. Hybrid CMOS/memristor crossbar structure for implementing Hopfield neural network. *Analog Integrated Circuits and Signal Processing*. 2020. pp.1-13.
- [33] Nikonov D., Csaba G., Porod W., Shibata T., Voils D., Hammerstrom D., Young I. Bourianoff G. Coupled-Oscillator Associative Memory Array Operation for Pattern Recognition. *IEEE Journal on Exploratory Solid-State Computation Devices and Circuits*. 2015. V. 1, pp. 85-93.
- [34] Csaba G., Porod W. Coupled oscillators for computing: A review and perspective. 2020. *Appl. Phys. Rev.* 7, 011302 (2020); doi: 10.1063/1.5120412
- [35] Raychowdhury A., Parihar A., Smith G. Narayanan V., Csaba G.,



- Jerry M., Porod W., Datta S. Computing with Networks of Oscillatory Dynamical Systems. *Proceedings of the IEEE* 2019. V 107, pp.73–89.
- [36] Hsieh C. C., Chang Yao-Feng, Chen Y.-C. et al., Review of Recently Progress on Neural Electronics and Memcomputing Applications in Intrinsic SiO<sub>x</sub>-Based Resistive Switching Memory. Book Chapter: "Memristor and Memristive Neural Networks", ISBN: 978-953-51-5481-5. InTech. 2018. <http://dx.doi.org/10.5772/intechopen.68530>
- [37] Wang Y., Wang G., Shen, Y., Iu H. A. Memristor Neural Network Using Synaptic Plasticity and Its Associative Memory. *Circuits, Systems, and Signal Processing*. 2020. pp.1-16.
- [38] Luo B., Li Y., Liu D., Yang Z., Zhu, Y. Adaptive synchronization of memristor-based neural networks with discontinuous activations. *Neurocomputing*. 13th November 2019. pp.1-31
- [39] Yang L., Zeng Z., Shi X. A memristor-based neural network circuit with synchronous weight adjustment. *Neurocomputing*. 18th July 2019. pp.1-11.
- [40] Chua L.O., Kim, H., Sah, M., Roska, T., Yang, C. Memristor Bridge Synapses. *Proceedings of the IEEE*. 2011. V.100, N.6, pp. 2061-2070.
- [41] Secco J., Poggio M., Corinto F. Supervised neural networks with memristor binary synapses. *International Journal of Circuit Theory and Applications*. 2018. V.46. N.1. pp.1-13.
- [42] Arthur J., Boahen K. Silicon-Neuron Design: A Dynamical Systems Approach. *IEEE Transactions on Circuits and Systems I: Regular Papers*. 2011. V. 58, pp. 1034- 1043. DOI: 10.1109/TCSI.2010.2089556.
- [43] Andrew S., Cassidy A., Merolla P., Arthur J. et al. Cognitive Computing Building Block: A Versatile and Efficient Digital Neuron Model for Neurosynaptic Cores. *International Joint Conference on Neural Networks*. 2013. pp.1-10. DOI:10.1109/IJCNN.2013.6707077
- [44] Tsubone T., Saito T. Manifold piecewise constant systems and chaos. *IEICE Trans. Fundamentals*. 1999. E82-A, N 8, pp.1619-1626.
- [45] Matsuda C., Torikai H. A Novel Generalized PWC Neuron Model: Theoretical Analyses and Efficient Design of Bifurcation Mechanisms of Bursting. *IEEE Transactions On Circuits and Systems II: Express Briefs*. 2012. V. 11, N. 4.
- [46] Yamashita Y., Torikai H., Theoretical Analysis for Efficient Design of a Piecewise Constant Spiking Neuron Model. *IEEE Transactions On Circuits and Systems II: Express Briefs*. 2014. V. 61, N. 1, pp 54-58.
- [47] Mitsubori K., Saito T. Dependent Switched Capacitor Chaos Generator and Its Synchronization. *IEEE Transactions On Circuits and Systems. I*. 1997. V. 44, N. 12, pp. 1122–1128.
- [48] Tsubone T., Saito T., Inaba N. Design of an analog chaos-generating circuit using piecewise-constant dynamics. *Prog. Theor. Exp. Phys.*, 053A01, 2016.
- [49] Rakitin.V., Rusakov S. Coupled Piecewise Constant Memristor based Reactance-less Oscillators. *IEEE East-West Design & Test Symposium (EWDTS)*, 2020.
- [50] Rakitin.V., Rusakov S. Memristor based Oscillators with Controlled Threshold Parameters. *European Conference on Circuit Theory and Design (ECCTD)*, 2020.
- [51] Yang J., Strukov D., Stewart D. Memristive devices for computing.

- Nature Nanotechnology.2013. V.8. N.1. pp.13-24. pp. 588-590, doi: 10.1109/ECCTD.2009.5275054.
- [52] Vourkas I., Sirakoulis G. Memristor-Based Nanoelectronic Computing Circuits and Architectures. Springer 2016 DOI 10.1007/978-3-319-22647-7.
- [53] Burr G., Shelby R., Sebastian A., et al. Neuromorphic computing using non-volatile memory. Advances in Physics: X. 2017;2(1):89-124
- [54] Suri M., editor. Advances in Neuromorphic Hardware Exploiting Emerging Nanoscale Devices. Springer. 2017. 210 p. DOI 10.1007/978-81-322-3703-7
- [55] Liang H., Cheng H., Wei J., Zhang L., Yang L., Zhao Y., Guo H. Memristive Neural Networks: A Neuromorphic Paradigm for Extreme Learning Machine. IEEE Transactions on Emerging Topics in Computational Intelligence. 2019. V. 3, N.1, pp.15-23.
- [56] Wang W. Binary-oscillator Networks: Bridging a Gap Between Experimental and Abstract Modeling of Neural Networks. Neural Comput. 1996. N 8. pp. 319-39.
- [57] Joao V., Giacomini E., Qureshi Y., Zapater M., Tang, X, Kvatinsky, S., Atienza, D., Gaillardon P.-E. A Product Engine for Energy-Efficient Execution of Binary Neural Networks Using Resistive Memories. In: IFIP/IEEE International Conference on Very Large Scale Integration (VLSI-SoC). 2019. pp.1-6
- [58] Pham K., Nguyen T., Tran S., et. al. Memristor Binarized Neural Networks. Journal of Semiconductor Technology and Science (JSTS). 2018. V.18. N.5. pp.568-577
- [59] Elwakil A. S. and Ozoguz S., "A low frequency oscillator structure," 2009 European Conference on Circuit Theory and Design, Antalya, Turkey, 2009,
- [60] Zidan MA, Omran H, Radwan AG, Salama KN. Memristor-based reactance-less oscillator. Electronics Letters 2011; 47, pp. 1220–1221.
- [61] Azghadi R., Chen Y.-C., Eshraghian J. K., Chen, J., Lin C.-Y., Amirsoleimani, A., Chang Yao-Feng et al. Complementary metal-oxide semiconductor and memristive hardware for neuromorphic computing. Adv. Intell. Syst. 2:1900189. 2020. pp. 1-24. doi: 10.1002/aisy.201900189